(Received 6 February 2026, Accepted 25 March 2026, Scheduled 22 April 2026)

Design of Multi Band Filtering Antenna with Low Mutual Coupling Using Decoupling Network

Deepika Verma[1, *], Kiran K. Verma[1], and Chandan[2]

[1] *Dr. Ram Manohar Lohia Avadh University, Ayodhya, Uttar Pradesh, India*
[2] *Madan Mohan Malaviya University of Technology, Gorakhpur, Uttar Pradesh, India*

ABSTRACT: This paper presents the design of a compact multi-band filtered MIMO antenna, whereby a UWB antenna is converted into a tri-band antenna by adding two stubs-loaded band-notch filters (SLBNFs). The notch structures tactfully quiet undesired frequency bands and permit three clean operating bands likely to be utilized in S-band and C-band wireless systems. A 2×2 MIMO system is proposed using a centrally located decoupling network to regulate the distribution of surface currents, which achieves over 25 dB of isolation in all operating bands. The fractional bandwidth of the antenna in the first band (2.0–2.6 GHz), second band (3.48–3.82 GHz), and third band (5.68–6.42 GHz) are 16%, 9.3%, and 12.23%, respectively. The peak gains in the corresponding operating bands are 2.8 dB, 4.1 dB, and 5 dB, respectively. The proposed design is suitable for the present-day S- and C-band communication systems and multi-standard wireless devices due to its selective multi-band response, better isolation, and compact structure.

1. INTRODUCTION

Recent studies show that multi-band and frequency-selective antenna configurations are being developed as a result of the market's insatiable demand for compact multifunctional antennas that are small enough to fit several wireless standards [1–3]. Ultra-wideband (UWB) antennas have numerous applications, including radar systems, biomedical sensors, ground-penetrating radar, indoor location systems, and short-range wireless communications. UWB antennas are power efficient, provide high data rates, and have a large bandwidth [4]. However, the continuous broadband radiation of conventional UWB antennas often leads to interference with licensed wireless services like WiMAX, WLAN, 5G NR sub-6 GHz [5, 6], and satellite bands, thereby limiting their practical deployment. To address this issue, filtered antennas have become the industry standard. Integrated with a notch filter or frequency-selective structure, these antennas provide dual functions and are compact [7, 8].

Several antenna engineering techniques have been developed to realize multi-band or frequency-selective responses. Common approaches include incorporating resonant slots, such as U-shaped, C-shaped, E-shaped, or complementary split-ring structures into the radiator or ground plane to introduce rejection bands [3, 6, 9, 10]. Defected Ground Structures (DGSs) have been broadly implemented to modify current distribution and achieve band-notch characteristics or bandwidth enhancement [11–13]. Parasitic resonators, stubs, and ring-shaped elements provide additional resonances, enabling multi-band operation in compact geometries [3, 13, 14]. Electromagnetic bandgap (EBG) structures further offer sharp filtering responses and effective suppression of surface waves [15, 16], while multi-mode excitation techniques exploit orthogonal or higher-order resonant modes to support multiple well-defined operating bands [17, 18].

Although these techniques are effective for single-element antennas, integrating them into compact multiple-input multiple-output (MIMO) systems remains challenging due to increased electromagnetic coupling between closely spaced radiators [12, 19, 20]. Various antenna topologies, including monopole antennas [21–25], compact patch antennas [26, 27], and slot-embedded designs [28], have been proposed for multi-band wireless systems. Multi-branch and reconfigurable antenna architectures have also been explored to accommodate diverse wireless standards, such as WLAN, WiMAX, 4G, and 5G NR [29–31]. Despite substantial progress, several research gaps persist in the design of multi-band filtered MIMO antennas. Prior works have explored diverse strategies, including Bandpass Stub-Loaded Resonators [3, 7], Uniplanar Microstrip-Inspired Filtering Antennas [8], designs featuring absorptive band-edge radiation nulls [32], EBG and split-ring-resonator-based filtering antennas [15, 16], multipath coupling structures [33], filtering patch antennas inspired by bandpass filter prototypes [34], quad-mode stub-loaded resonators [35], antennas utilizing multiple coupling paths between resonant and spurious modes [36], shared substrate integrated waveguide (SIW) cavity-based filtering antennas [37], multiple-mode resonator filtering antennas [38], and filtering antennas employing U-shaped slots [9].

To overcome the drawbacks, this research suggests a compact multi-band filtered MIMO antenna that uses twin notch filters that selectively suppress unwanted frequency areas to convert a conventional UWB radiator into a tri-band structure. To greatly lessen mutual coupling and redistribute the surface

* Corresponding author: Deepika Verma (deepikaverma609@gmail.com).

current, a centrally located decoupling network is fitted among the antenna elements. Three distinct operating bands appropriate for S-band and C-band wireless applications are produced by this integrated design method, which also achieves isolation exceeding 25 dB across all bands. The suggested antenna maintains a compact and planar structure while providing constant radiation properties, wide fractional bandwidths, and steady gain. These characteristics make the design ideal for cutting-edge wireless systems, such as future portable communication platforms, multi-standard communication modules, radar sensors, and Internet of Things (IoT) devices.

2. PROPOSED FILTERED ANTENNA DESIGNING

2.1. Discussion of MIMO Antenna Design Structure

The proposed multiband filtered MIMO antenna with a 2×2 configuration is displayed in Fig. 1. The detailed design parameters are listed in Table 1. Fig. 1(a) displays the front view of the 2×2 MIMO design. Four identical, modified circular radiating patches are arranged orthogonally to achieve pattern diversity. Each element is excited using a microstrip feed line, and two arc-shaped resonant structures are placed near the feeding region to function as dual band-stop (notch) filters [3, 6, 9, 10]. With these resonators, the original UWB radiator is transformed into a tri-band antenna. The elements are positioned symmetrically, which helps maintain balanced radiation characteristics and reduces envelope correlation. Fig. 1(b) presents the rear view, where a centrally located cross-shaped decoupling structure, implemented with via interconnections, is used to improve isolation [12, 14].

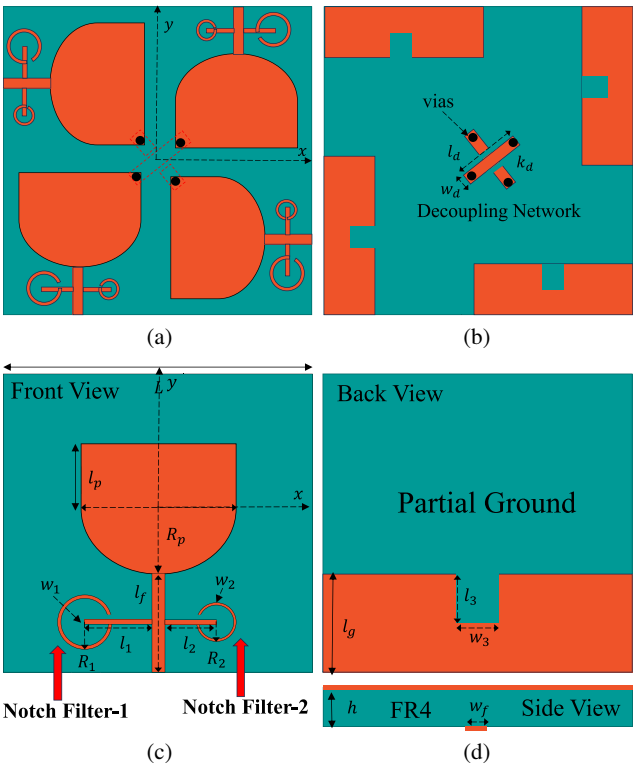

FIGURE 1. The proposed MIMO antenna: (a) a front view of the 2×2 MIMO antenna, (b) rear view of the 2×2 MIMO antenna, (c) front view of a single antenna including notch filters, and (d) rear view of the single antenna element.

TABLE 1. MIMO design parameters.

Parameters	Values (in mm)	Parameters	Values (in mm)
L	50	l_1	5
l_p	9	l_2	3
R_p	20	l_3	4
l_g	16.5	w_1	0.5
w_f	3	w_2	0.27
l_f	16.56	w_3	4.5
R_1	2.1	R_2	1.65
l_d	15	w_d	1
h	1.6	k_d	0.2

In Fig. 1(c), we show the front view of a single antenna element with its geometrical specifications, radiating patch, feed line, and two notch filters, labeled as Notch Filter 1 and Notch Filter 2. These filters remove certain frequencies from the original UWB response [3, 6], enabling the antenna to operate in three desired bands: S-band, lower C-band, and upper C-band. The partial ground plane shown in Fig. 1(d) assists radiation pattern stabilization, bandwidth modification, and impedance matching [11, 13].

2.2. Designing UWB Antenna

The geometrical design of the antenna is presented in Fig. 2. In the front view, the radiator features a modified circular patch with length l_p and radius R_p. A microstrip feed line with length l_f runs parallel to it to stimulate the radiating surface and facilitate broad-spectrum impedance matching. A partial ground plane, which is critical for bandwidth enhancement and impedance matching, is shown in the back view. The ground plane contains a rectangular aperture of dimensions $l_g \times l_3$ and breadth w_3, which serves to optimize current flow. The side view depicts an FR4 substrate of height h and width w_f. In summation, these design elements contribute to a sustained wide-spectrum impedance bandwidth.

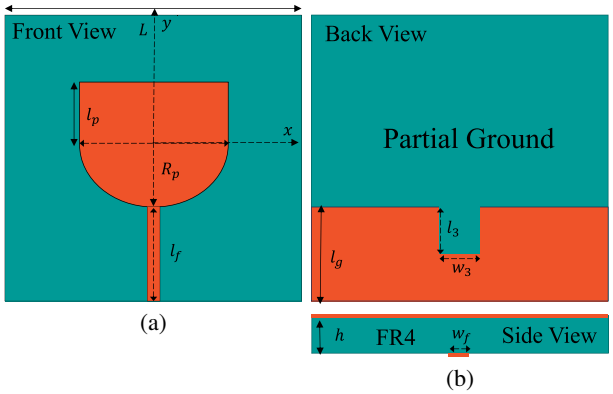

FIGURE 2. Structure of the UWB antenna: (a) front view, (b) back view.

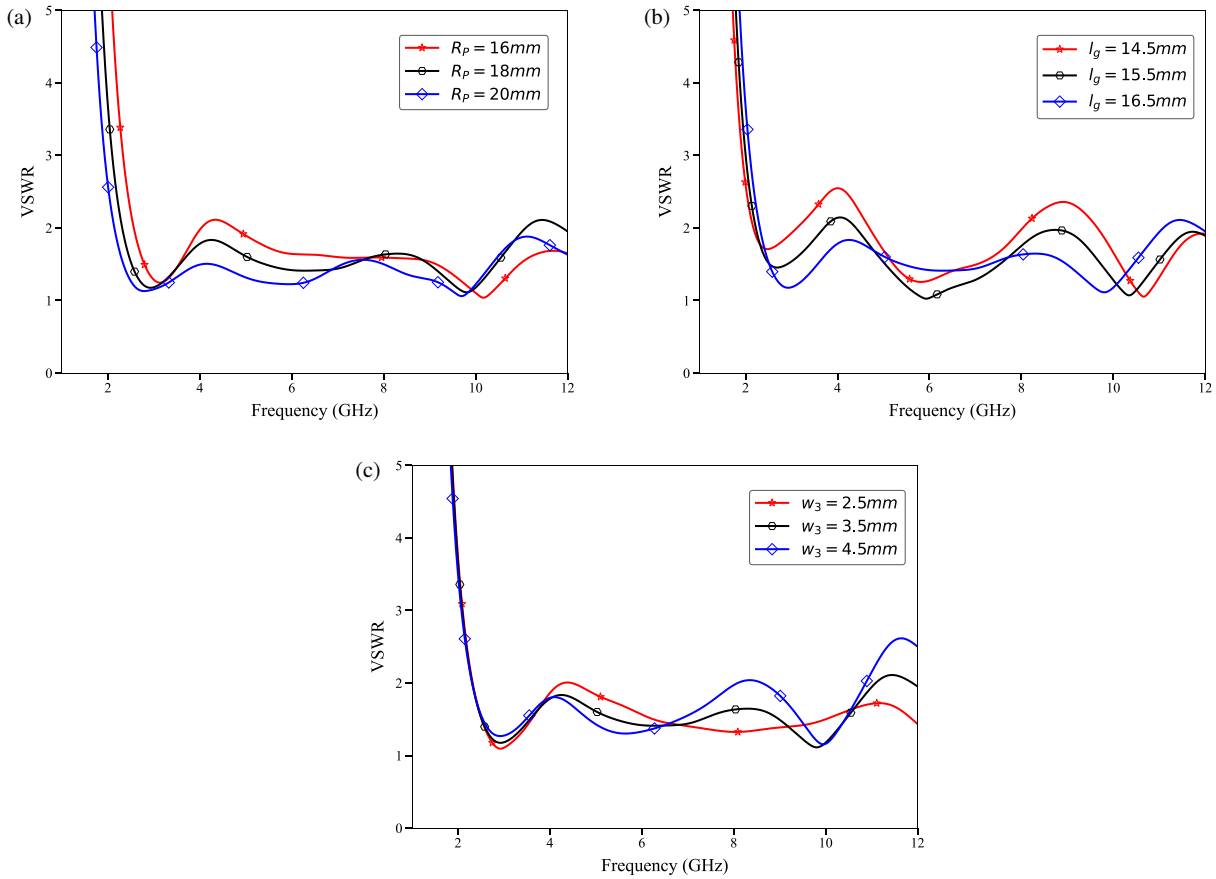

FIGURE 3. VSWR plots for parametric study: (a) variation of R_p, (b) variation of l_g, and (c) variation of w_3.

A parametric study on voltage standing wave ratio (VSWR) for three antenna parameters — patch radius R_p, ground length l_g, and slot width w_3 — is presented in Fig. 3.

2.2.1. Effect of Patch Radius R_p

In Fig. 3(a), as R_p increases, resonant modes move to lower frequencies. The antenna with $R_p = 20$ mm achieves the most stable impedance matching in the 3–6 GHz range, and $R_p = 16$ mm has a higher VSWR, confirming that patch radius has a strong impact on resonance behavior.

2.2.2. Effect of Ground Length l_g

From Fig. 3(b), $l_g = 15.5$ mm gives the best matching. Smaller ground length reduces return-current cancellation, and larger ground length shifts the resonances, confirming that l_g is sensitive to UWB performance.

2.2.3. Effect of Slot Width w_3

In Fig. 3(c), increasing w_3 modifies the ground current distribution. A slot width of 3.5 mm gives the best VSWR performance, and 4.5 mm gives poor matching at higher frequencies, making slot width a fine-tuning parameter.

2.3. Designing Notch Filter

The design layout for the dual band-notch filters integrated with the UWB antenna is presented in Fig. 4 [3, 6]. Two circular resonators are placed symmetrically with respect to the feed line, constituting Notch Filter 1 and Notch Filter 2. The first is defined by parameters w_1, R_1, and l_1, and the second by w_2, R_2, and l_2. Each resonator creates a resonant current loop that eliminates certain interference bands present in the UWB spectrum. Notch Filter 1 (approximately 3–4 GHz) and Notch Filter 2 (approximately 4.5–5.0 GHz) eliminate interference signals in the

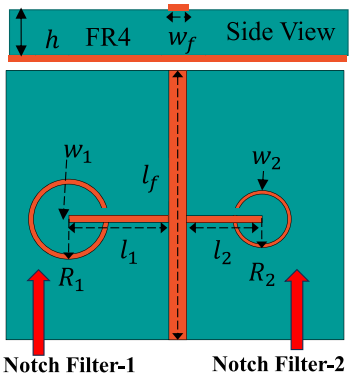

FIGURE 4. Layout of the dual band-notch filter structure showing Notch Filter 1 (parameters w_1, R_1, l_1) and Notch Filter 2 (parameters w_2, R_2, l_2) integrated with the UWB antenna feed line.

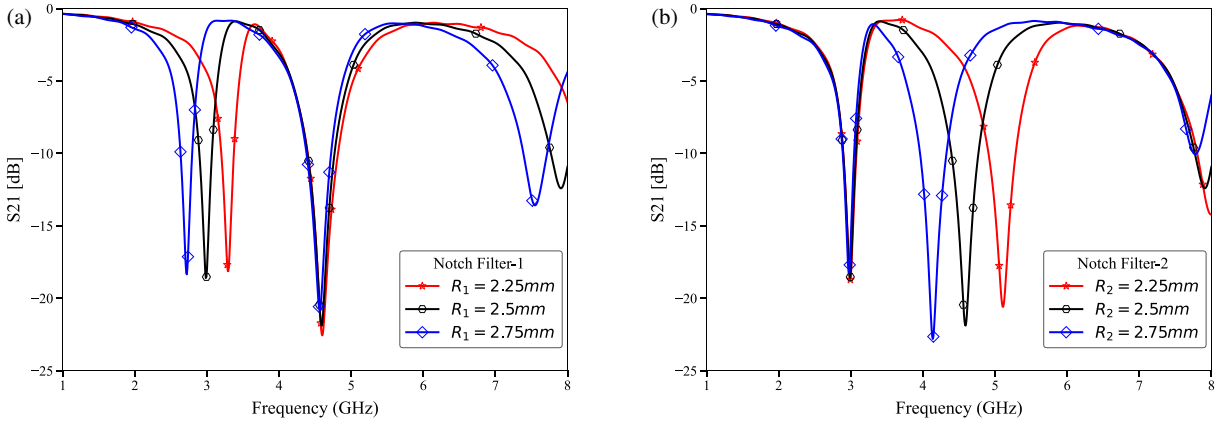

FIGURE 5. Parametric study of the notch filter radii: (a) S_{21} for varying R_1 (Notch Filter 1), (b) S_{21} for varying R_2 (Notch Filter 2).

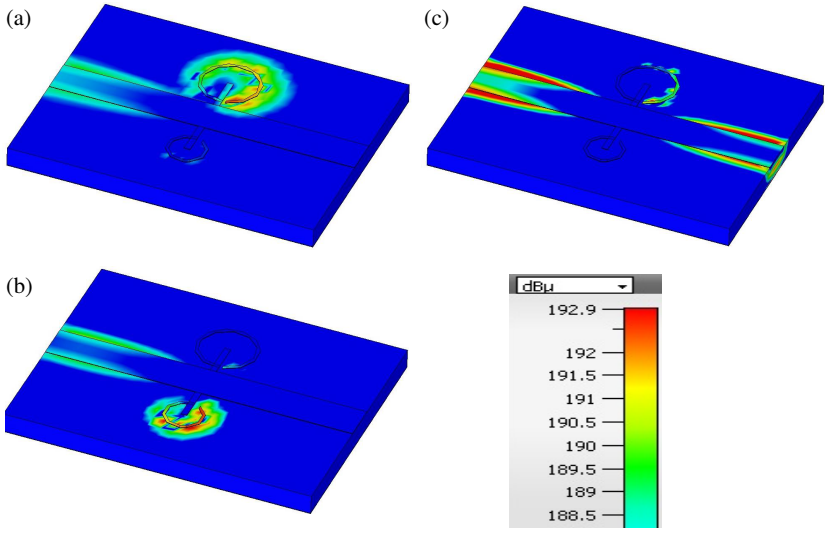

FIGURE 6. Electric field distribution illustrating the notch filter mechanism: (a) at $f = 3$ GHz corresponding to Notch Filter 1 stopband, (b) at $f = 4.58$ GHz corresponding to Notch Filter 2 stopband, (c) at $f = 3.5$ GHz representing the passband condition.

lower and upper bands, respectively [5, 6]. Notch frequencies are mainly determined by R_1 and R_2, which control the effective electrical length of the current loop. The selective dual-band rejection is illustrated in Fig. 4.

Figure 5 presents the S_{21} responses for different values of the resonator radii, showing how changes in R_1 and R_2 independently shift the corresponding stopband frequencies. The electric field distributions validating the notch mechanism are shown in Fig. 6.

2.3.1. Effect of Radius R_1 on Notch Filter 1

Figure 5(a) shows variations in R_1: 2.25 mm, 2.50 mm, and 2.75 mm. The notch frequency decreases as R_1 increases due to the longer effective electrical path. Strong suppression ($S_{21} < -20$ dB) confirms effective filtering.

2.3.2. Effects of the Radius R_2 on Notch Filter 2

Figure 5(b) shows that increasing R_2 from 1.50 mm to 1.80 mm shifts the upper notch to a lower frequency and improves suppression, confirming that R_2 controls the tuning of the upper stopband.

The electric field distributions in Fig. 6 are presented at three representative frequencies to validate the filtering mechanism. At $f = 3$ GHz (Fig. 6(a)), a strong electric-field concentration is observed around Notch Filter 1, confirming that the resonator is actively confining energy and creating the lower stopband. At $f = 4.58$ GHz (Fig. 6(b)), the fields are mainly localized around Notch Filter 2, verifying effective suppression of the upper interference band. By contrast, at $f = 3.5$ GHz (Fig. 6(c)), energy propagates smoothly along the feed line without localization near either resonator, corresponding to the passband condition. These field plots confirm that each resonator suppresses its intended frequency band while maintaining stable passband behaviour.

2.4. UWB Antenna Loaded Dual Band Notch Filter

In Fig. 7(a), the VSWR response of the unmodified UWB antenna remains below 2 across the entire operating band, confirming stable wideband impedance matching. After introduc-

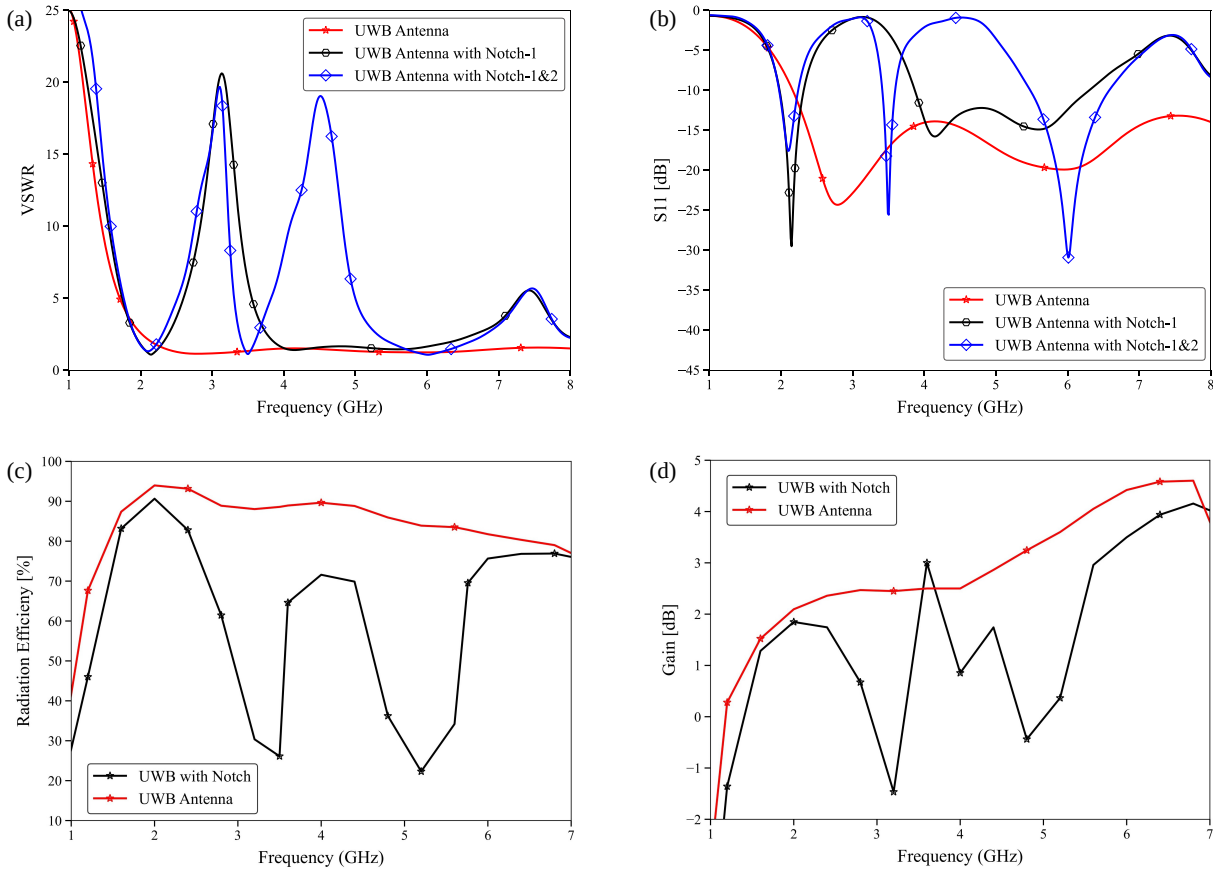

FIGURE 7. Comparison of the UWB antenna, the UWB antenna with a single band notch, and the UWB antenna with dual-band notches: (a) VSWR plots, (b) S_{11} plots, (c) radiation efficiency, and (d) gain.

ing the first notch filter, a distinct VSWR peak appears near 3 GHz. When both notch filters are incorporated, two pronounced peaks are observed around 3 GHz and 4.58 GHz, confirming that the dual-notch configuration successfully rejects both undesired frequency ranges.

The S_{11} responses in Fig. 7(b) show deep notches at the same frequencies, demonstrating rejection levels below -20 dB. These comparisons verify that the resonators provide controlled impedance behavior to realize stopbands without degrading the overall UWB performance [3, 6].

Figure 7(c) shows the radiation efficiency versus frequency. The UWB antenna exhibits consistently high efficiency, typically 78–94% across the operating band. The UWB notch antenna exhibits efficiency dips at the notch frequencies, where radiation is suppressed; beyond the notch regions, the efficiency closely follows that of the original UWB antenna.

Figure 7(d) shows the gain versus frequency. The UWB antenna shows a gradual increase in gain with frequency, reaching approximately 4–4.5 dB at higher frequencies. The notch UWB antenna exhibits gain drops at the notch bands, while good gain performance is maintained outside those bands.

Figure 8 provides electric-field visualizations for the dual-notch antenna. At $f_1 = 2.1$ GHz (Fig. 8(a)), the field is smoothly distributed over the radiating region representing passband radiation. At $f_2 = 3.5$ GHz (Fig. 8(b)) and $f_3 = 5.8$ GHz (Fig. 8(c)), uniform field flow confirms that neither notch filter is activated. In contrast, localized field concentration around Notch Filter 1 at $f_{n1} = 3$ GHz (Fig. 8(d)) and around Notch Filter 2 at $f_{n2} = 4.58$ GHz (Fig. 8(e)) confirms that the resonators trap electromagnetic energy at their notch frequencies and generate deep stopbands.

3. MIMO ANTENNA DESIGNING

3.1. Designing MIMO Antenna

Figure 9 shows the S-parameters of the proposed MIMO antenna [12, 14]. As seen in Fig. 9(a), without the decoupling network, the antenna elements have good impedance matching, but S_{21} and S_{31} are significant, exceeding -18 dB, which limits MIMO performance. In Fig. 9(b), after integrating the central decoupling network, S_{21} and S_{31} are reduced to below -25 dB in most operating bands, while S_{11} and S_{41} remain unaffected. These results show that the decoupling network successfully redirects surface currents, achieving higher isolation without disturbing individual element impedance matching. Once the decoupling network is added, a small frequency shift and bandwidth reduction occur in the third operating band due to changes in current distribution and effective electrical length introduced by the decoupling stubs and vias.

Figure 10 shows the electric field distribution of the proposed MIMO antenna, illustrating the influence of the decoupling structure. Without the decoupling network, the elec-

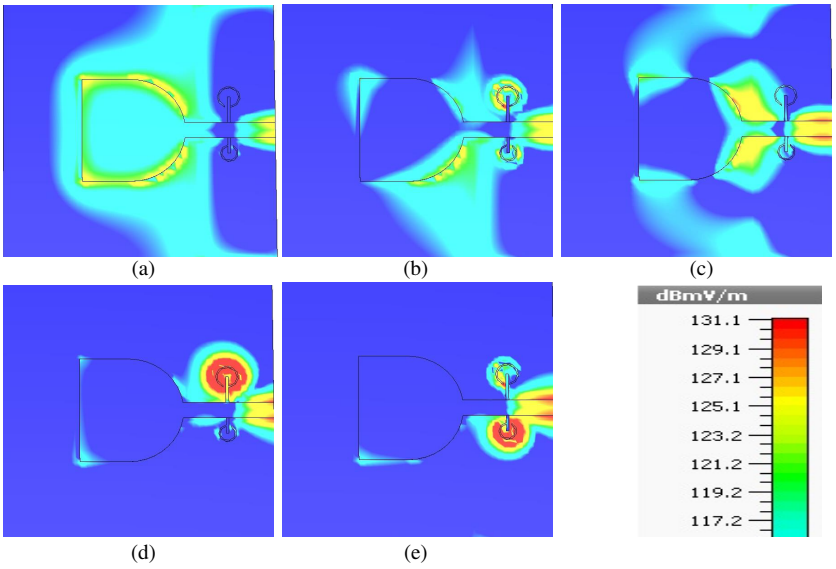

FIGURE 8. Electric field distribution of the dual-band-notch UWB antenna: (a) first passband at $f_1 = 2.1$ GHz, (b) second passband at $f_2 = 3.5$ GHz, (c) third passband at $f_3 = 5.8$ GHz, (d) first notch band at $f_{n1} = 3$ GHz, and (e) second notch band at $f_{n2} = 4.58$ GHz.

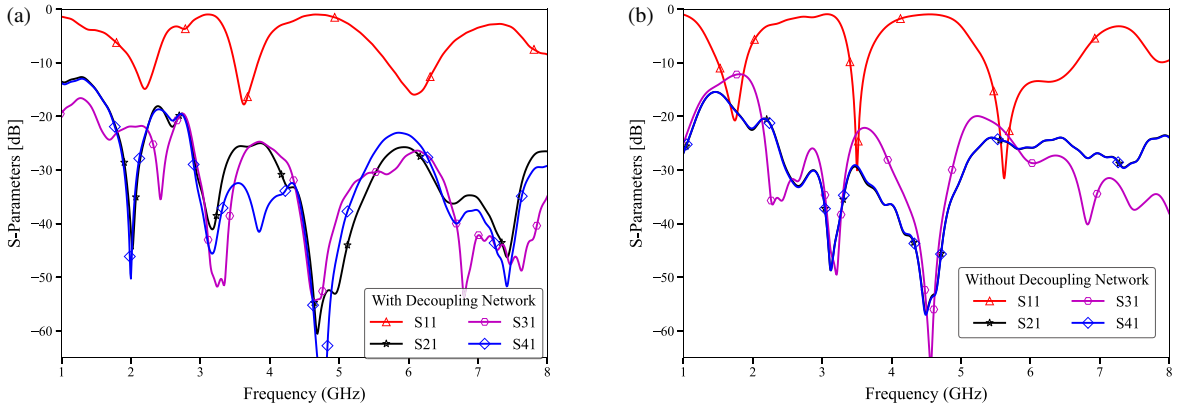

FIGURE 9. S-parameters of the MIMO antenna: (a) without a decoupling network, (b) with a decoupling network.

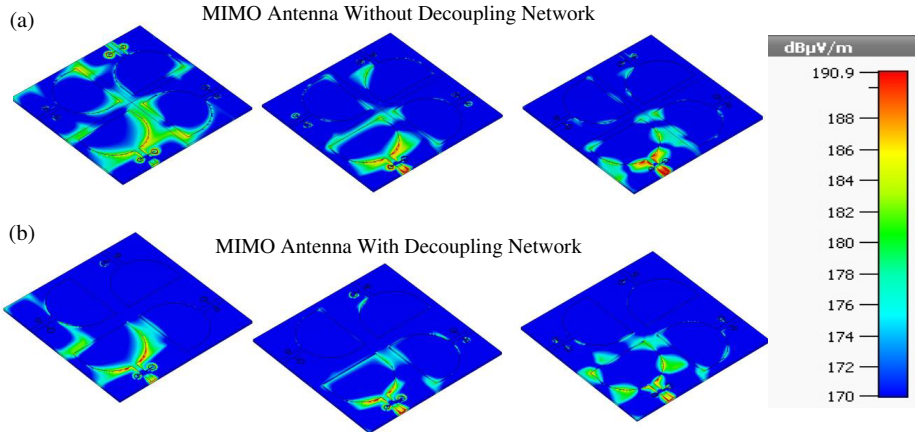

FIGURE 10. Electric field distribution of the MIMO antenna: (a) without the decoupling network, (b) with the decoupling network.

tric fields are dispersed throughout the substrate and ground plane, indicating strong coupling between radiators, consistent with the elevated S_{21} and S_{31} in Fig. 9(a). With the decoupling network, the electric fields are concentrated around the individual antenna elements with little leakage to neighbouring elements. The proposed decoupling structure uses compact microstrip stubs with vias to create a counteracting coupling field that effectively cancels induced currents between adjacent

elements, preventing surface-wave propagation and improving inter-element isolation with minimal effect on impedance matching or radiation properties.

4. MIMO ANTENNA HARDWARE DESIGN AND MEASUREMENT

The manufactured prototype of the proposed MIMO antenna, built on an FR4 substrate ($\varepsilon_r = 4.3$, $t = 1.6$ mm) using standard chemical etching, is shown in Fig. 11 [2, 12]. The antenna was designed and simulated in Computer Simulation Technology (CST) Microwave Studio. The simulation layout is converted to a Digitized Frequency Modulated (DFM) photomask, transferred to a copper-clad FR4 sheet, and the excess copper removed by etching in ferric chloride ($FeCl_3$).

Figure 11(a) shows the front layer with the etched radiating patches, and Fig. 11(b) shows the back layer with the ground plane and decoupling network. For experimental validation, the antenna is evaluated using a Vector Network Analyzer (VNA) as shown in Fig. 11(b), where only one port is excited, and the remaining ports are terminated with 50 Ω matched loads. Gain and radiation patterns are assessed in an anechoic chamber, as shown in Fig. 11(c).

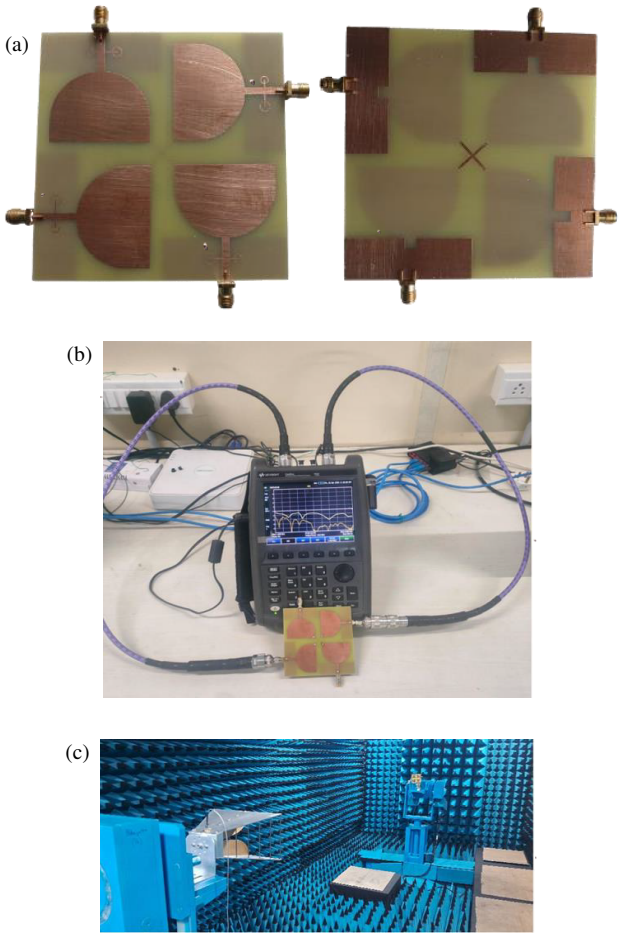

FIGURE 11. Fabricated prototype and measurement setup: (a) front view (left) and back view (right) of the fabricated antenna, (b) Vector Network Analyzer (VNA) measurement setup, (c) anechoic chamber setup.

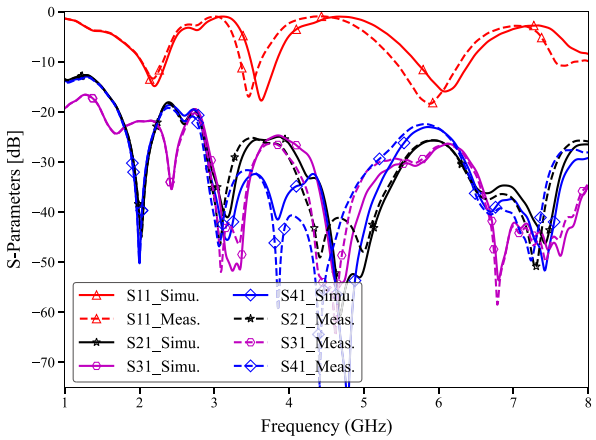

FIGURE 12. Simulated and measured S-parameters of the proposed MIMO antenna.

In Fig. 12, the simulated and measured S-parameters are compared. The measured S_{11} closely agrees with the simulation, confirming proper fabrication and impedance matching. The measured S_{21}, S_{31}, and S_{41} are below -20 dB across almost all operating bands, confirming the positive impact of the decoupling network on inter-element isolation [12, 14]. Minor differences are attributed to soldered SMA connectors, FR4 tolerances, and fabrication imperfections.

The simulated and measured gains of the proposed MIMO antenna are shown in Fig. 13. The measured peak gain is in the range of 2–4 dB and shows good agreement with simulations. Minor discrepancies are attributed to measurement alignment, substrate uniformity, and connector/cable losses.

Figure 13(b) shows the simulated and measured E-plane radiation patterns at 2.1 GHz, 3.5 GHz, and 5.8 GHz for both co-polarization and cross-polarization. Measured results closely agree with the simulation at all three bands. The co-polarized component dominates with suppressed cross-polarization, demonstrating stable radiation performance across the operating bands.

4.1. Proposed MIMO Antenna Diversity Performance

In a MIMO system, antenna diversity defines the ability of multiple elements to provide low-correlation signal paths, improved link resiliency, and enhanced channel capacity. The diversity performance of the proposed MIMO antenna is evaluated using three metrics.

4.1.1. Envelope Correlation Coefficient (ECC)

ECC is calculated using far-field 3D radiation patterns to estimate diversity behavior in practical multipath environments. The far-field approach captures true correlation by combining pattern polarization and power distribution [39–41]:

$$\mathrm{ECC}_{12} = \frac{\left|\iint_0^{4\pi}\left[F^{(1)}(\theta,\phi)\times F^{(2)}(\theta,\phi)d\Omega\right]\right|^2}{\left(\iint_0^{4\pi}\left|F^{(1)}(\theta,\phi)\right|^2 d\Omega\right)\left(\iint_0^{4\pi}\left|F^{(2)}(\theta,\phi)\right|^2 d\Omega\right)} \quad (1)$$

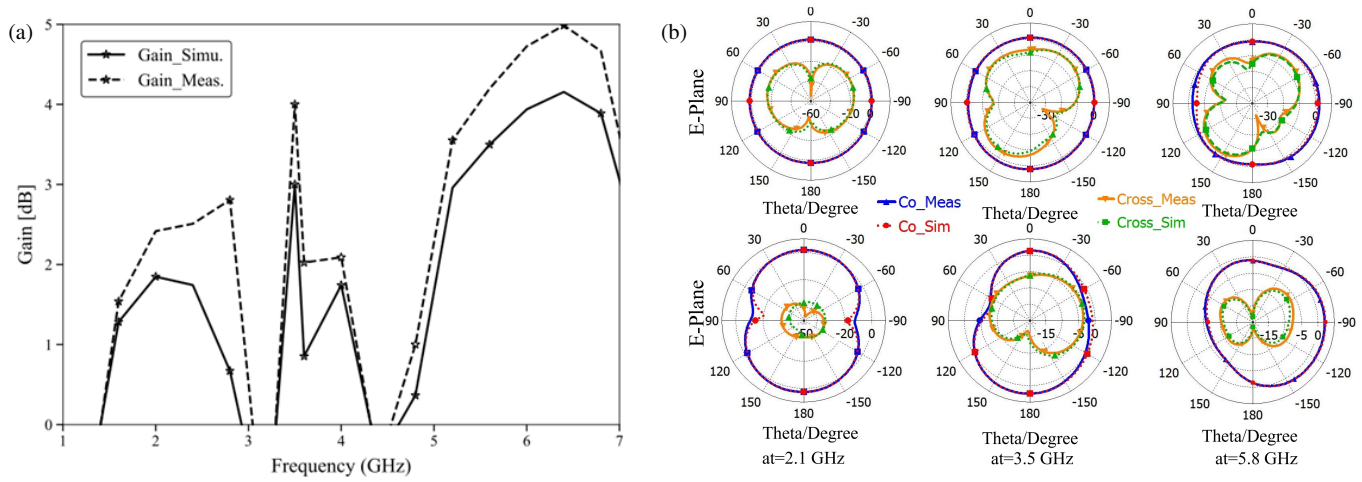

FIGURE 13. Simulated and measured gains of the MIMO antenna: (a) broadband gain versus frequency, (b) E-plane radiation patterns at 2.1 GHz, 3.5 GHz, and 5.8 GHz.

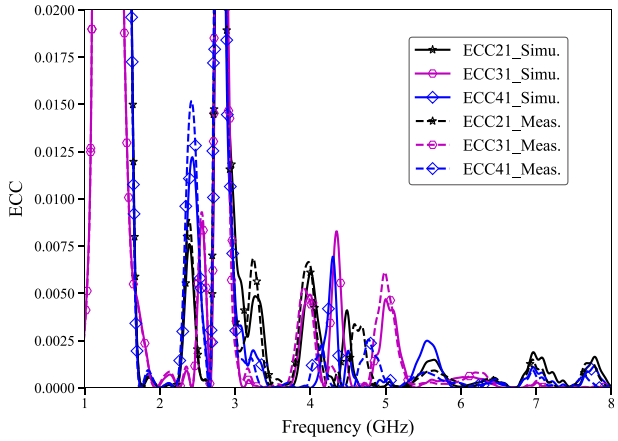

FIGURE 14. Simulated and measured envelope correlation coefficients (ECCs).

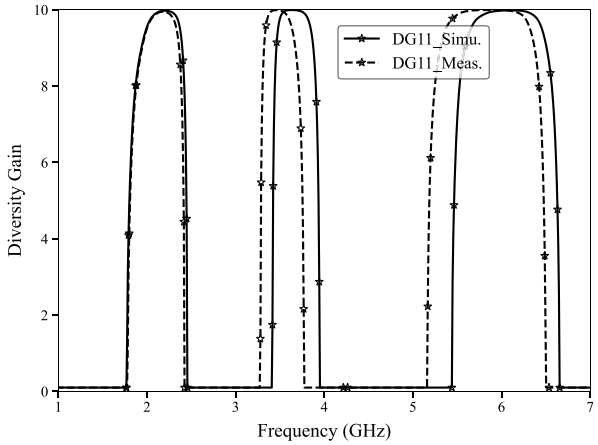

FIGURE 15. Simulated and measured diversity gains (DGs).

where $F^{(1)}(\theta,\phi)$ and $F^{(2)}(\theta,\phi)$ are the complex far-field vectors of antenna elements 1 and 2. A uniform angular power spectrum $P(\theta,\phi)=1$ is assumed.

4.1.2. Diversity Gain (DG)

DG quantifies the improvement in signal reliability achieved through diversity [39–41]:

$$\mathrm{DG} = 10\sqrt{1-\mathrm{ECC}^2} \tag{2}$$

For an ideal uncorrelated MIMO system, DG ≈ 10 dB.

4.1.3. Channel Capacity Loss (CCL)

CCL quantifies the reduction in achievable data rate due to correlation among antenna elements [42, 43]:

$$\mathrm{CCL} = -\log_2 \det(A) \tag{3}$$

$$A = \begin{bmatrix} \rho_{11} & \rho_{12} \\ \rho_{21} & \rho_{22} \end{bmatrix} \tag{4}$$

$$\rho_{ii} = 1 - \left(|S_{ii}|^2 + |S_{ij}|^2\right) \tag{5}$$

$$\rho_{ij} = 1 - \left(S_{ii}^* S_{ij} + S_{ji}^* S_{jj}\right) \tag{6}$$

A CCL below 0.4 bits/s/Hz indicates negligible capacity degradation.

Figure 14 shows the simulated and measured ECCs for different antenna element pairs. Across all operating bands, ECC is consistently below 0.01, well within the requirement of ECC < 0.02. This confirms the effectiveness of the decoupling network in providing high diversity performance across the S- and C-band frequency ranges.

Figure 15 shows the simulated and measured DGs of the proposed MIMO antenna. DG remains close to 10 dB across all operating bands, confirming solid diversity improvement and high reliability in multipath environments. Good agreement is observed between simulated and measured DGs.

Figure 16 shows the simulated and measured CCLs of the proposed MIMO antenna. CCL remains below 0.4 bits/s/Hz in all main operating bands, confirming high channel capacity with minimal degradation due to mutual coupling. A comparison with related works is provided in Table 2, which demon-

TABLE 2. Related research work.

Ref.	Band (GHz)	Size (λ_0)	Isolation (dB)	Bandwidth (%)	Notch (GHz)	Method	Gain (dBi)
This work	2.1, 3.5, 5.8	0.35×0.35	25	16, 9.3, 12.23	3 and 4.58	Stubs-loaded notch filter	2.8, 4.1, 5
[9]	11.8	0.48×0.47	-	11.84	3.3–3.6, 5.15–6	Filtering antenna with U-shaped slots	5
[16]	3–11	0.42×0.55	15	114	3.5, 5.5, 8.5	EBG	-
[37]	4.25, 5.11	0.99×0.99	-	2.8, 4.7	-	Shared SIW cavity	7.93, 7.44
[39]	2.33–16	0.6×0.6	20	-	3.28–3.8, 5.05–5.9, 7.78–8.51	Alpha-shaped coupled line with SLR	5.1
[43]	mm-Wave	-	high	-	-	Parasitic element-loaded dual-band	-
[44]	S band	0.52×0.52	27	7.7, 14	-	Filtering elements	7.7, 7.8
[45]	S, C band	0.27×0.33	-	-	-	Stubs embedded in feedline	-

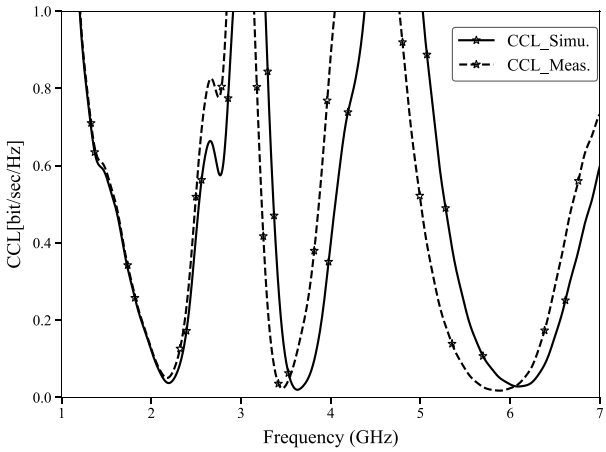

FIGURE 16. Simulated and measured channel capacity losses (CCLs).

strates that the proposed antenna achieves competitive isolation and compact footprint relative to prior designs.

5. CONCLUSION

This work presents the design, fabrication, and measurement of a compact multiband MIMO antenna incorporating two band-notch filters and a centrally located decoupling network [2, 12, 14]. By embedding stub-loaded resonant structures within the original UWB radiator, three operating bands are realized with fractional bandwidths of 16% (2.0–2.6 GHz), 9.3% (3.48–3.82 GHz), and 12.23% (5.68–6.42 GHz) [3, 6–8]. Peak gains of 2.8 dB, 4.1 dB, and 5 dB are achieved with stable radiation behaviour. The central decoupling structure provides inter-element isolation exceeding 25 dB without degrading individual element impedance matching [12, 14]. A prototype fabricated on an FR4 substrate shows good agreement between simulated and measured S-parameters, gains, and radiation patterns. Diversity analysis confirms ECC < 0.02, DG ≈ 10 dB, and CCL < 0.4 bits/s/Hz, demonstrating excellent MIMO performance [39–43]. The proposed antenna is well-suited for compact IoT platforms and multi-standard wireless devices operating in the S- and C-bands.

REFERENCES

[1] Nayak, P., S. Verma, and P. Kumar, "A study of ultrawideband (UWB) antenna design for cognitive radio applications," *arXiv preprint arXiv:2106.15272*, 2021.

[2] Ahmad, S., S. Khan, B. Manzoor, M. Soruri, M. Alibakhshikenari, M. Dalarsson, and F. Falcone, "A compact CPW-fed ultra-wideband multi-input-multi-output (MIMO) antenna for wireless communication networks," *IEEE Access*, Vol. 10, 25 278–25 289, 2022.

[3] Modak, S., S. Daasari, P. P. Shome, and T. Khan, "Switchable/tunable band-notched characteristics in UWB and UWB-MIMO antennas: A comprehensive review," *Wireless Personal Communications*, Vol. 128, No. 3, 2131–2154, 2023.

[4] Faouri, Y., S. Ahmad, S. Naseer, K. Alhammami, N. Awad, A. Ghaffar, and M. I. Hussein, "Compact super wideband frequency diversity hexagonal shaped monopole antenna with switchable rejection band," *IEEE Access*, Vol. 10, 42 321–42 333, 2022.

[5] Nan, J., J. Zhao, M. Gao, W. Yang, M. Wang, and H. Xie, "A compact 8-states frequency reconfigurable UWB antenna," *IEEE Access*, Vol. 9, 144 257–144 263, 2021.

[6] Devana, V. N. K. R., E. K. Kumari, K. S. Chakradhar, P. K. Sharma, D. R. Devi, C. M. Kumar, V. D. Raj, and D. R. Prasad, "A novel foot-shaped elliptically embedded patch-ultra wide band antenna with quadruple band notch characteristics verified by characteristic mode analysis," *International Journal of Communication Systems*, Vol. 35, No. 15, e5284, 2022.

[7] Duan, Z., S. Shen, and G. Wen, "A compact tri-band filtering antenna system for 5G sub-6 GHz applications," *IEEE Transactions on Antennas and Propagation*, Vol. 70, No. 11, 11 097–11 102, 2022.

[8] Chen, C., "A compact wideband endfire filtering antenna inspired by a uniplanar microstrip antenna," *IEEE Antennas and Wireless Propagation Letters*, Vol. 21, No. 4, 853–857, 2022.

[9] Yin, J.-Y., T.-L. Bai, J.-Y. Deng, J. Ren, D. Sun, Y. Zhang, and L.-X. Guo, "Wideband single-layer substrate integrated waveguide filtering antenna with U-shaped slots," *IEEE Antennas and Wireless Propagation Letters*, Vol. 20, No. 9, 1726–1730, 2021.

[10] Yuan, H., F.-C. Chen, and Q.-X. Chu, "A wideband and high gain dual-polarized filtering antenna based on multiple patches," *IEEE Transactions on Antennas and Propagation*, Vol. 70, No. 10, 9843–9848, 2022.

[11] Mahmoud, K. R. and A. M. Montaser, "Design of compact mm-Wave tunable filtenna using capacitor loaded trapezoid slots in ground plane for 5G router applications," *IEEE Access*, Vol. 8, 27 715–27 723, 2020.

[12] Abdullah, M., S. H. Kiani, N. Shoaib, T. Ali, H. Elmannai, A. D. Algarni, and U. F. Khattak, "An eight element wideband DGS MIMO antenna system for 5G handheld devices," *IEEE Access*, Vol. 12, 141 476–141 488, 2024.

[13] Shome, P. P., T. Khan, S. K. Koul, and Y. M. M. Antar, "Two decades of UWB filter technology: Advances and emerging challenges in the design of UWB bandpass filters," *IEEE Microwave Magazine*, Vol. 22, No. 8, 32–51, 2021.

[14] Kumar, R., M. Sharma, L. Matta, P. Kaur, N. Saluja, S. Malhotra, M. Singh, G. S. Saini, and S. Singh, "Mutual coupling reduction techniques for UWB-MIMO antenna for band notch characteristics: A comprehensive review," *Wireless Personal Communications*, Vol. 131, No. 2, 1207–1247, 2023.

[15] Arora, S., S. Sharma, R. Anand, and G. Shrivastva, "Miniaturized pentagon-shaped planar monopole antenna for ultra-wideband applications," *Progress In Electromagnetics Research C*, Vol. 133, 195–208, 2023.

[16] Thakur, E., N. Jaglan, A. Gupta, and A. J. A. Al-Gburi, "Multi-band notched circular polarized MIMO antenna for ultra-wideband applications," *Progress In Electromagnetics Research M*, Vol. 125, 87–95, 2024.

[17] Zehforoosh, Y., "Evaluation of a novel hook-shaped multiband monopole antenna based on the AHP method," *IET Communications*, Vol. 16, No. 3, 266–273, Jan. 2022.

[18] Balakrishnan, N. A. and E. C. Britto, "Compact SCSRR-based quad-band antenna for Bluetooth, WiMAX, WLAN, and fixed-satellite services," *International Journal of Communication Systems*, Vol. 36, No. 16, e5586, Aug. 2023.

[19] Hussain, M., W. A. Awan, M. S. Alzaidi, and D. H. Elkamchouchi, "Self-decoupled tri band MIMO antenna operating over ISM, WLAN and C-band for 5G applications," *Heliyon*, Vol. 9, No. 7, e17404, Jul. 2023.

[20] Aliqab, K., A. Armghan, M. Alsharari, and M. H. Aly, "Highly decoupled and high gain conformal two-port MIMO antenna for V2X communications," *Alexandria Engineering Journal*, Vol. 74, 599–610, Jul. 2023.

[21] Verma, D., K. K. Verma, and Chandan, "A compact E shaped rectangular monopole antenna for WLAN and WiMAX applications," in *International Conference on Electronics, Computer, Physical and Chemical Sciences*, 513–518, CRC Press, 2024.

[22] Chandan, G. Bharti, T. Srivastava, and B. S. Rai, "Dual band monopole antenna for WLAN 2.4/5.2/5.8 with truncated ground," *AIP Conference Proceedings*, Vol. 1952, No. 1, 020036, 2018.

[23] Singh, K. P., Chandan, and G. Bharti, "A compact tri band monopole antenna with L stub for WLAN/WiMAX applications," in *2018 3rd International Innovative Applications of Computational Intelligence on Power, Energy and Controls with their Impact on Humanity (CIPECH)*, 1–5, Ghaziabad, India, 2018.

[24] Chandan, and B. S. Rai, "Bandwidth enhancement of Wang shape microstrip patch antenna for wireless system," in *2014 Fourth International Conference on Communication Systems and Network Technologies*, 11–15, Bhopal, India, 2014.

[25] Bhasker, M. K., Chandan, and R. K. Prasad, "Design of monopole antenna with defected ground for WLAN application," in *2016 International Conference on Emerging Trends in Electrical Electronics & Sustainable Energy Systems (ICETEESES)*, 91–94, Sultanpur, India, 2016.

[26] Choudhary, S., Y. Sharma, S. Kumar, and Chandan, "Dual circular-inverted L planar patch antenna for different wireless applications," in *Cyber Physical Systems*, 737–743, ser. Lecture Notes in Electrical Engineering (LNEE), Springer, 2021.

[27] Kushwaha, M. S., Chandan, and R. K. Prasad, "Improvement of bandwidth of microstrip patch antenna by multiple notches," in *Proceedings of the Conference on Advances in Communication and Control Systems (CAC2S 2013)*, 245–248, Uttar Pradesh, India, Apr. 2013.

[28] Srivatava, K., Chandan, and A. K. Singh, "Dual-band miniaturised T-shaped centre slot monopole antenna for WiMAX/GPS communication application," in *International Conference on Electronics, Computer, Physical and Chemical Sciences*, 62–71, CRC Press, 2024.

[29] Vinayagam, K. and R. Natarajan, "Design of multiband frequency reconfigurable antenna with switchable polarization states," *Microwave and Optical Technology Letters*, Vol. 66, No. 2, e34057, Feb. 2024.

[30] Xu, Y., Z. Zhang, A. Wang, and J. Hou, "Design of three multibranch microstrip antennas compatible with WiMAX/WiFi/4G/5G NR for coal mine applications," *Microwave and Optical Technology Letters*, Vol. 65, No. 3, 892–900, 2023.

[31] Sultan, K., M. Ikram, and N. Nguyen-Trong, "Integrated large-frequency-ratio dual-band tapered slot with monopole antenna for 4G/5G/B5G," *Microwave and Optical Technology Letters*, Vol. 66, No. 1, e33499, 2024.

[32] Li, J.-F., C.-X. Mao, D.-L. Wu, L.-H. Ye, and G. Zhang, "A dual-beam wideband filtering patch antenna with absorptive band-edge radiation nulls," *IEEE Transactions on Antennas and Propagation*, Vol. 69, No. 12, 8926–8931, 2021.

[33] Chen, B.-J., X.-S. Yang, and B.-Z. Wang, "A compact high-selectivity wideband filtering antenna with multipath coupling structure," *IEEE Antennas and Wireless Propagation Letters*, Vol. 21, No. 8, 1654–1658, 2022.

[34] Ji, S., Y. Dong, and Y. Fan, "Bandpass filter prototype inspired filtering patch antenna/array," *IEEE Transactions on Antennas and Propagation*, Vol. 70, No. 5, 3297–3307, 2022.

[35] Zhang, G., A. Basit, M. I. Khan, A. Daraz, N. Saqib, and F. Zubir, "Multi frequency controllable in-band suppressions in a broad bandwidth microstrip filter design for 5G Wi-Fi and satellite communication systems utilizing a quad-mode stub-loaded resonator," *Micromachines*, Vol. 14, No. 4, 866, 2023.

[36] Zhao, D., F. Lin, H. Sun, and X. Y. Zhang, "A miniaturized dual-band SIW filtering antenna with improved out-of-band suppression," *IEEE Transactions on Antennas and Propagation*, Vol. 70, No. 1, 126–134, 2022.

[37] Ji, S., Y. Dong, and Y. Fan, "Low-profile dual-band filtering antenna with a shared SIW cavity," *IEEE Antennas and Wireless Propagation Letters*, Vol. 20, No. 10, 2053–2057, 2021.

[38] Lin, H., S.-W. Wong, K.-W. Tam, Y. Li, K. Ngai, C.-H. Chio, and Y. He, "Filtenna-filter-filtenna-based FSS with simultaneous wide passband and wide out-of-band rejection using multiple-mode resonators," *IEEE Transactions on Antennas and Propagation*, Vol. 71, No. 6, 5046–5056, 2023.

[39] El-Gendy, M. S., M. M. M. Ali, E. B. Thompson, and I. Ashraf, "Triple-band notched ultra-wideband microstrip MIMO antenna with bluetooth band," *Sensors*, Vol. 23, No. 9, 4475, 2023.

[40] Abubakar, H. S., Z. Zhao, M. E. Munir, W. U. K. Tareen, B. Wang, S. H. Kiani, and T. Ali, "Enhanced smartphone connectivity: Dual-band MIMO antenna with high isolation and low ECC," *Physica Scripta*, Vol. 99, No. 6, 065524, 2024.

[41] Sritongnuan, P., P. Thitimahatthanakusol, N. Supreeyatitikul, and J. Konpang, "Dual-port bi-directional CP metasurface-integrated MIMO antenna for Wi-Fi 7 full-duplex communications," *Engineering Science and Technology, an International Journal*, Vol. 68, 102103, 2025.

[42] Esmail, B. A. and S. Koziel, "High isolation metamaterial-based dual-band MIMO antenna for 5G millimeter-wave applications," *AEU — International Journal of Electronics and Communications*, Vol. 158, 154470, 2023.

[43] Hussain, M., W. A. Awan, E. M. Ali, M. S. Alzaidi, M. Alsharef, D. H. Elkamchouchi, A. Alzahrani, and M. F. A. Sree, "Isolation improvement of parasitic element-loaded dual-band MIMO antenna for mm-Wave applications," *Micromachines*, Vol. 13, No. 11, 1918, 2022.

[44] Yang, S. J., W. Duan, Y. Y. Liu, H. Ye, H. Yang, and X. Y. Zhang, "Compact dual-band base-station antenna using filtering elements," *IEEE Transactions on Antennas and Propagation*, Vol. 70, No. 8, 7106–7111, 2022.

[45] Ellis, M. S., P. Arthur, A. R. Ahmed, J. J. Kponyo, B. Andoh-Mensah, and B. John, "Design and circuit analysis of a single and dual band-notched UWB antenna using vertical stubs embedded in feedline," *Heliyon*, Vol. 7, No. 12, e08554, 2021.